# Ni–Pt/H-Y zeolite catalysts for hydroisomerization of *n*-hexane and *n*-heptane

I. Eswaramoorthi [a,*] and N. Lingappan [b]

[a] *Department of Chemistry, College of Engineering, Anna University, Chennai-600025, India*
[b] *Science and Humanities Division, Madras Institute of Technology, Anna University, Chennai-600044, India*

Received 6 November 2002; accepted 27 January 2003

Ni–Pt/H-Y zeolite catalysts with different Ni contents were prepared and applied to the hydroisomerization of *n*-hexane and *n*-heptane in the temperature range 225–375 °C. ESCA studies show the complete reduction of Ni species up to 0.3 wt% Ni addition over 0.1 wt% Pt/H-Y and further addition leads to the occurrence of unreduced nickel species as $NiAl_2O_4$. A TEM study shows the formation of bimetallic (Ni–Pt) particles of nanoscale size and the average particle size is found to increase with increasing Ni loading. Acidity measurements by $NH_3$-TPD and pyridine-adsorbed FTIR spectroscopy show the increasing occupation of acid sites by the added nickel when increasing the nickel loading. The catalytic activity of Ni–Pt/H-Y zeolite and Pt/H-Y catalysts was compared and it was found that addition of Ni up to 0.3 wt% increases the *n*-hexane and *n*-heptane conversion, multibranched isomer selectivity and sustainability of the catalysts due to better metal–acid synergism, complete reduction of Ni species and the formation of catalytically active Ni–Pt bimetallic particles. Further Ni addition leads to a decrease in conversion and multibranched isomer selectivity and an increase in the cracked products, which may be due to the presence of unreduced Ni species and pore blockage by larger-sized bimetallic particles formed.

**KEY WORDS:** *n*-hexane; *n*-heptane; hydroisomerization; Y-zeolite; platinum; nickel.

## 1. Introduction

More stringent limits on the amount of aromatics included in gasoline have resulted in a renewed interest in the skeletal isomerization of *n*-alkanes with a view to using the branched isomers as octane-enhancing components. Efforts have been made to develop catalysts that are effective at lower temperature, since lower temperature favors branched isomers at equilibrium. The progression has been from $Pt/Al_2O_3$ to Pt/chlorided $Al_2O_3$, which are active for isomerization at 450–500 and 350–400 °C, respectively. Recently, Pt/H-zeolite catalysts [1,2], which are active in the range 200–250 °C have been extensively studied [3,4]. Also, Pt/sulfated $ZrO_2$ [5],$Pt/WO_x$–$ZrO_2$ [6] and related materials have been used as isomerization catalysts. Weisz [7] proposed a classical bifunctional mechanism for alkane isomerization over solid acid catalysts. According to him, isomerization proceeds via dehydrogenation–isomerization–hydrogenation in which isomerization is the rate-limiting step. Various mechanisms have been proposed in contrast to Weisz's classical mechanism for *n*-alkane isomerization. A bond shift rearrangement involving a $\alpha,\alpha,\gamma$-triadsorbed species [8], 1,3-diadsorbed species [9], penta-coordinated carbonium ion [10] and protonated cyclopropane (PCP) structure as intermediates [11] for *n*-alkane isomerization have been reported. Also, a hydride transfer type [5], acid-catalysed chain reaction [12] and dimerization–cracking [13] mechanism were observed over various Pt/acidic supports. Noble metals supported on zeolites such as Y, USHY [14], mazzite [15], mordenite and $\beta$ [3] are considered as potential commercial catalysts for $C_5/C_6$ paraffin isomerization reactions. Also, very recently Pt-supported silicoaluminophosphates [16–19] and mesoporous molecular sieves [20,21] have been used for *n*-alkane hydroisomerization.

Generally, enhanced activity and selectivity in isomerization reactions were observed over bimetallic bifunctional catalysts compared with monometallic bifunctional catalysts [14]. Ward [22] reported that the property of the first dispersed metal is influenced by the addition of the second metal due to the formation of metallic clusters. Nickel was first introduced as the second metal by Vazquez *et al.* [23], who studied *n*-heptane isomerization and cracking over Ni–Mo/H-Y zeolite. They found that the Ni/(Ni + Mo) atomic ratio of the catalyst had a strong influence on the activity. Maximum activity in *n*-heptane conversion was observed over a catalyst with Ni/(Ni + Mo) ≈ 0.5. Also, the introduction of a small amount of Pd to Pt/H-$\beta$ and Pt/H-Y zeolite catalysts enhances the activity and isomerization selectivity in *n*-heptane isomerization [14]. Further, it was observed that the introduction of Pd not only increases the Pt dispersion and stability of the catalysts, but also suppresses the undesired hydrogenolysis and cracking activity. Similarly, Jao *et al.* [24] studied *n*-hexane and *n*-heptane isomerization over 0.2 wt% Pt and varying amounts (0, 0.26, 0.5 and 1.5 wt%) of Ni on H-mordenite. They observed that the addition of Ni up to 0.5 wt% not

* To whom correspondence should be addressed.
E-mail: eswarchem@hotmail.com

1011-372X/03/0400-0133/0 

only enhances the conversion and rate of branched isomer formation but also suppresses fuel gas formation. The improved catalytic performance by the addition of Ni was accounted for in terms of an increase in the number of metallic sites/acid sites ($N_M/N_A$) ratio.

Malyala *et al.* [25] compared Ni and Ni–Pt supported on Y-zeolite for acetophenone hydrogenation and found that Ni–Pt/Y-zeolite was more active, selective and stable than Ni/H-Y zeolite catalysts. Further they concluded that a strong synergistic effect of Pt in the Ni–Pt bimetallic catalyst is responsible for the higher activity observed. Jordao *et al.* [26] studied *n*-hexane isomerization over 1 or 2 wt% Ni and Pt in different proportions on HUSY and found that the bimetallic Ni–Pt/HUSY containing 20–30% Pt showed higher activity and selectivity to high-octane branched isomers than monometallic (Ni or Pt) catalysts. In our previous study [27], *n*-hexane hydroisomerization was carried out over 0.1 wt% Pt and varying amounts (0, 0.1, 0.3 and 0.5 wt%) of Ni-impregnated H-$\beta$ and H-mordenite catalysts. It was observed that the addition of Ni up to 0.3 and 0.1 wt% over 0.1 wt% Pt-loaded $\beta$ and mordenite, respectively, enhances the conversion, dimethyl butane (DMB) selectivity and sustainability of the catalyst. Further addition of Ni leads to a decreasing trend in activity, DMB selectivity and stability and enhances the undesired cracking. The improved catalytic activity by Ni addition was accounted for in terms of better metal–acid balance and formation of catalytically active bimetallic (Ni–Pt) particles of nanometer scale. Similarly, *n*-hexane conversion, isomerization and DMB selectivity was found to increase with Ni addition up to 0.4 wt% over 0.2 wt% Pt-loaded SAPO-5 and SAPO-11 due to better metal–acid synergism [28]. Further Ni addition led to a decrease in the activity of the catalysts. Reports [29,30] are available on Ni-containing isomerization catalysts. There is a report [31] on alloy formation between Ni and Pt with a common f.c.c. structure suggesting some potential bimetallic interactions between these two metals and hence allowing them to be catalytically active in hydrocarbon reforming reactions. Few reports are available in the literature about Ni addition as the second metal to Pt, but the Ni concentration is kept in a fairly high range. Hence, in the present study, Ni is introduced as the second metal in a lower concentration range (i) to modify the catalytic properties of Pt/H-Y zeolite in *n*-hexane and *n*-heptane hydroisomerization and (ii) to study the isomer selectivity and ratio among the isomers of hexane and heptane at various reaction temperatures.

## 2. Experimental

### 2.1. Catalyst preparation

The sodium form of zeolite-Y ($SiO_2/Al_2O_3 = 6$) was supplied by United Catalyst India Ltd, India. H-Y was obtained by repeated ion exchange with aqueous 1 M $NH_4Cl$ solution followed by calcination at 550 °C for 6 h. A part of the H-Y was loaded with 0.1 wt% Pt by incipient wetness impregnation (IWI) and designated as catalyst $A_1$. Catalysts $A_2$, $A_3$ and $A_4$ were obtained after impregnation of $A_1$ with 0.1, 0.3 and 0.5 wt% Ni. Catalyst $A_5$ was obtained by ion exchanging with 0.1 Pt and 0.3 Ni and $A_6$ by impregnating 0.4 wt% Ni on H-Y. Aqueous solutions of chloroplatinic acid (Sisco Research Laboratory; $2 \times 10^{-4}$ g Pt/ml) and nickel nitrate (Central Drug House; $5 \times 10^{-4}$ g Ni/ml) were used as sources of Pt and Ni, respectively. The metal-loaded catalysts were dried at 120 °C for 12 h.

### 2.2. Characterization

The dried metal-loaded catalysts were activated at 550 °C for 3 h under a nitrogen atmosphere and reduced at 475 °C for 6–7 h under flowing hydrogen (30 ml/min/g). The reduced catalysts were used for further characterization as well as for catalytic studies. The states of Ni and Pt in catalysts $A_3$ and $A_4$ were determined by ESCA. The ESCA spectra were acquired with a surface analysis system (ESCA LAB-MK11, VG Scientific) using Mg$K\alpha$ radiation (1253.6 eV) with pass energy of 50 eV. All the catalyst samples were insulators with a very small amount of carbonaceous impurity on their surfaces. The charging effect was corrected by setting the C 1*s* transition at 284.6 eV. Calcination and reduction were carried out in the catalyst preparation chamber, and the catalysts could be moved to the analysis chamber without exposure to air. During the spectral acquisition the pressure of the analysis chamber was maintained at better than $1 \times 10^{-7}$ torr. Transmission electron microscopy (TEM) measurements for catalysts $A_3$ and $A_4$ were carried out using a JEOL 200 kV electron microscope. Catalyst sample powders were dispersed on to "holy carbon" coated grids, which were then introduced to the microscope column, which was evacuated to less than $1 \times 10^{-6}$ torr. Specimens were enlarged using thin photographic paper and the sizes of metal particles visible in the photographs were measured manually and averaged.

The total acidity of the catalysts was measured by TPD of ammonia by a TGA method following the experimental procedure reported in our previous studies [27,28]. Instead of ammonia, adsorption was carried out with pyridine vapor and the FTIR spectra were recorded for catalysts $A_1$, $A_3$ and $A_4$ using a KBr pellet technique [28] in absorbance mode with a Nicolet (AVATAR) spectrometer. The BET surface area measurements for all the above catalysts were carried out using a Sorptomatic 1990 CE instrument following the BET procedure using nitrogen as adsorbant at liquid nitrogen temperature.

### 2.3. Catalytic studies

Reduced catalysts (1.5 g each) were packed in a fixed-bed continuous down-flow quartz reactor placed in a

tabular electric furnace. After activation at 550 °C for 3 h, the reaction was carried out from 225 to 375 °C in steps of 50 °C. The reactants *n*-hexane and *n*-heptane were separately fed into the reactor by a syringe pump at a predetermined flow rate. The LHSV of both *n*-hexane and *n*-heptane in all the catalytic runs was kept at 1.33/h. Pure hydrogen gas (20 ml/min/g) was also passed along with the reactant for all the catalytic runs. The products were collected at a time interval of 1 h under ice-cold conditions and were analyzed by gas chromatography (HP5890) using a FID. The identification of the products was done by GC-MS (Shimadzu QP 5000). The material balance calculation showed that more than 95% of the feed was recovered as products.

## 3. Results and discussion

### 3.1. Characterization

The ESCA spectra of Ni and Pt in catalysts $A_3$ and $A_4$ are shown in figure 1. In the case of Pt, two sharp peaks are observed with binding energy values around 71.0 and 74.5 eV, which correspond to the core level Pt $4f_{7/2}$ and Pt $4f_{5/2}$ transitions, respectively. In the case of Ni, a peak observed at a binding energy of 852.3 eV is the indication of the presence of nickel in the metallic state (Ni metal: 852.3 eV; NiO: 853.3 eV; $NiAl_2O_4$: 857.2 eV in Phi ESCA data book). A broad peak observed for catalyst $A_4$ at a binding energy of 857.0 eV indicates the presence of $NiAl_2O_4$ from which the reduction of $Ni^{2+}$ to $Ni^0$ is very difficult as reported by Minchev *et al.* [32]. Narayanan [33] reported that the reduction of Ni in the zeolite system is difficult, with a marked amount of nickel remaining unreduced and multiple species of Ni being formed during reduction. Platinum-catalyzed reduction of $Ni^{2+}$ to $Ni^0$ in Ni–Pt/Y-zeolite catalysts was observed by Malyala *et al.* [25] from their XPS studies on Ni/Y-zeolite and Ni–Pt/Y-zeolite systems. In the present case also, the added Pt (0.1 wt%) facilitates the reduction of $Ni^{2+}$ up to 0.3 wt% and a further increase in Ni addition leads to the occurrence of unreduced Ni as $NiAl_2O_4$. Similar observations were made in our previous studies on Ni–Pt/H-$\beta$ and Ni–Pt/H-MOR [27] and Ni–Pt-loaded SAPO-5 and SAPO-11 [28] systems.

The TEM images of catalysts $A_3$ and $A_4$, which differ by 0.2 wt% Ni loading, are shown in figures 2(a) and 2(b), respectively. The black dots appearing on the support matrix are assumed as bimetallic particles consisting of Pt and Ni. Jao *et al.* [24] observed a decrease in Ni reduction temperature with increasing Pt concentration from their TPR study of Ni–Pt/H-MOR systems and presumed a catalytic reduction of Ni due to mobile platinum oxide particles colliding with each other by thermal migration. Further they concluded that the nickel oxide particles are catalytically reduced by prereduced Pt particles. The average particle sizes of catalyst $A_3$ and $A_4$ are found to be 5.23 and 8.3 nm, respectively. It is observed that the average particle size increases with increasing nickel addition which is similar to the observation made in our previous studies on Ni–Pt/H-$\beta$ and Ni–Pt/H-MOR [27] and Ni–Pt/SAPOs [28] systems. The size of these bimetallic particles may not be smaller than the pore size of zeolite-Y (7.4 Å). Further it is assumed that these particles may mainly be located outside the pores of zeolite due to thermal mobility as

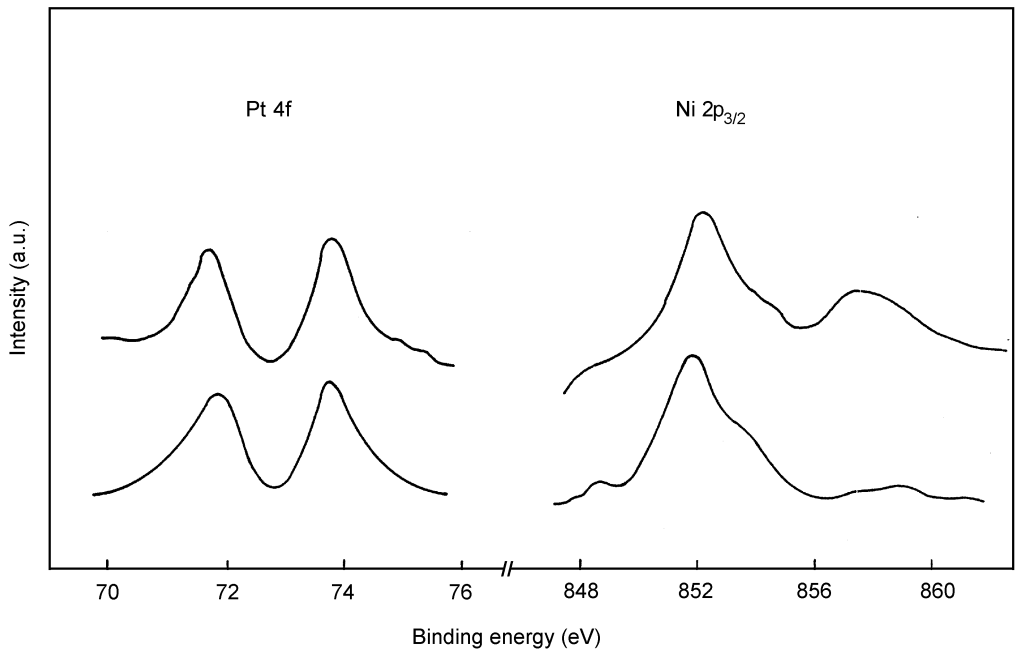


Figure 1. ESCA spectra of catalysts $A_3$ and $A_4$.

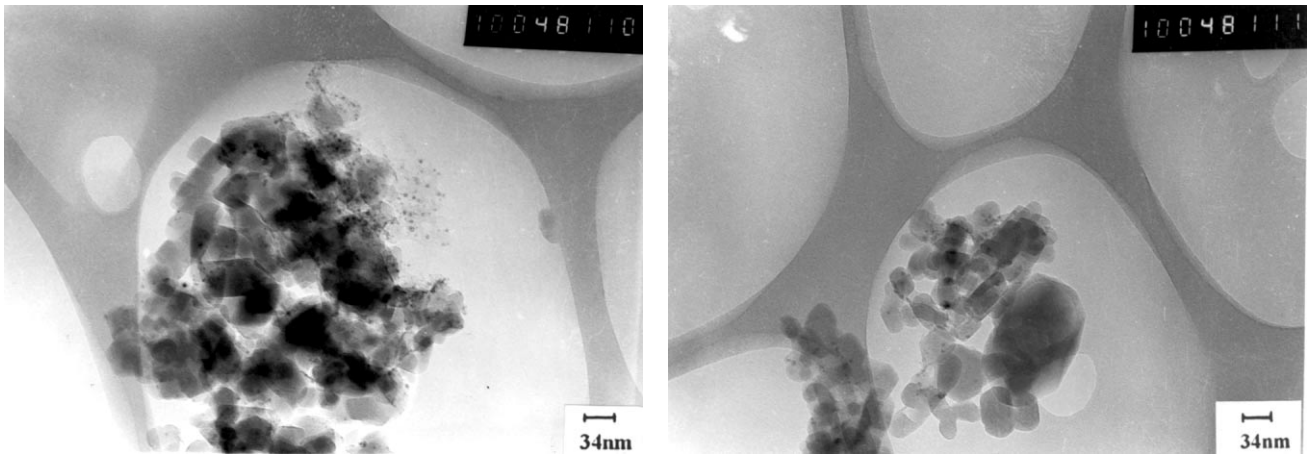


Figure 2. TEM images of catalyst (a) $A_3$ and (b) $A_4$.

reported by Canizares *et al.* [34] in Ni/H-mordenite catalysts.

The desorption of ammonia was carried out over the reduced catalysts by a TGA method and the amounts of desorbed ammonia are presented in table 1. There are two weight losses occurring at two different temperature ranges due to the desorption of absorbed ammonia. The first and second weight losses occurring in the range 150–180 and 270–300 °C, respectively, may be due to the desorption of ammonia absorbed on weak and strong acid sites, respectively. The amount of ammonia desorbed and the desorption temperature are considered as the indexes of total acidity and acid strength of catalysts [35]. It is observed from table 1 that the amount of ammonia desorbed at lower temperature is always found to be greater than that at higher temperature. Further, on increasing the Ni addition, the total acidity of the catalysts is found to decrease. The decrease in acidity with increasing nickel addition can be accounted for in terms of occupation of some of the acid sites by the added nickel species. On similar lines, the current observation is explained in terms of increasing occupation of acid sites of the supports by the increasing Ni addition, a process that may occur in parallel with Ni combining with Pt particles and the growth of Ni–Pt particles. The occupation of acid sites by added Ni has already been observed over Pt–Ni/H-MOR [24] and Ni–Pt-loaded H-$\beta$, H-MOR [27] and SAPOs [28] catalysts. The desorption temperature is not affected by the increasing Ni addition indicating the Ni addition does not affect the strength of acid sites. In the case of catalysts prepared by the ion exchange method and Ni-only-loaded catalysts, no significant change in total acidity is observed. The pyridine-adsorbed FTIR spectra (not shown) of catalysts $A_1$, $A_3$ and $A_4$ show a sharp peak around 1545 $cm^{-1}$ indicating the presence of pyridine adsorbed on Brønsted acid sites of zeolite-Y. The presence of Lewis acid sites is indicated by another sharp peak around 1455 $cm^{-1}$. The increasing addition of Ni did not affect the position of these peaks, but the intensity of the peaks was found to decrease indicating that the number of both Brønsted and Lewis acid sites decreases with increasing Ni loading. The decrease in the number of acid sites may be due to the occupation of acid sites by the added Ni species as observed in $NH_3$-TPD studies. A broad peak observed around 1490 $cm^{-1}$ indicates the physically adsorbed pyridine. The occupation of acid sites and increasing particle size by added nickel species is further supported by the

Table 1
Physicochemical properties of Ni–Pt/H-Y zeolite catalysts

| Catalyst | $SiO_2/Al_2O_3$ | Pt (wt%) | Ni (wt%) | Surface area ($m^2/g$) | $NH_3$-TPD (mmol/g) | | Total acidity (mmol/g) | Particle size (nm) from TEM [c] |
|---|---|---|---|---|---|---|---|---|
| | | | | | LT [a] peak | HT [b] peak | | |
| $A_1$ | 6 | 0.1 | – | 340 | 0.423 | 0.140 | 0.563 | nd |
| $A_2$ | 6 | 0.1 | 0.1 | 342 | 0.410 | 0.124 | 0.534 | nd |
| $A_3$ | 6 | 0.1 | 0.3 | 326 | 0.386 | 0.110 | 0.496 | 5.23 |
| $A_4$ | 6 | 0.1 | 0.5 | 311 | 0.357 | 0.104 | 0.461 | 8.3 |
| $A_5$ [d] | 6 | 0.1 | 0.3 | 328 | 0.364 | 0.117 | 0.481 | nd |
| $A_6$ | 6 | – | 0.4 | 335 | 0.346 | 0.126 | 0.472 | nd |

[a] Low-temperature peak.
[b] High-temperature peak.
[c] nd, not determined.
[d] Prepared by ion exchange method.

Table 2
Product distribution (wt%) and product ratios in *n*-hexane hydroisomerization at various temperatures (LHSV = 1.33/h, $H_2$ flow rate = 20 ml/min/g, mass of catalyst = 1.5 g, time on stream = 1 h)

| Product | 225 °C | | | | 275 °C | | | | 325 °C | | | | 375 °C | | | |
|---|---|---|---|---|---|---|---|---|---|---|---|---|---|---|---|---|
| | $A_1$ | $A_2$ | $A_3$ | $A_4$ | $A_1$ | $A_2$ | $A_3$ | $A_4$ | $A_1$ | $A_2$ | $A_3$ | $A_4$ | $A_1$ | $A_2$ | $A_3$ | $A_4$ |
| 2MP | 10.5 | 12.3 | 14.4 | 12.3 | 14.0 | 15.5 | 17.6 | 15.0 | 16.0 | 17.2 | 19.0 | 17.5 | 17.0 | 17.5 | 19.5 | 17.0 |
| 3MP | 5.6 | 6.7 | 8.3 | 7.5 | 8.0 | 10.2 | 12.8 | 10.6 | 8.5 | 10.0 | 12.5 | 11.5 | 10.2 | 12.0 | 14.5 | 12.3 |
| 22DMB | 1.0 | 2.0 | 2.5 | 1.5 | 2.6 | 4.2 | 5.6 | 4.7 | 4.5 | 5.8 | 7.6 | 5.0 | 5.0 | 7.0 | 9.3 | 8.5 |
| 23DMB | 1.0 | 1.5 | 1.5 | 1.0 | 2.2 | 3.0 | 4.5 | 3.3 | 3.3 | 4.5 | 5.8 | 4.7 | 4.0 | 5.7 | 6.7 | 5.2 |
| Cracked products | 2.5 | 3.0 | 3.3 | 4.2 | 4.7 | 5.3 | 6.0 | 7.0 | 6.5 | 7.0 | 7.3 | 8.5 | 8.0 | 8.5 | 8.5 | 10.2 |
| Conversion (wt%) | 20.6 | 25.5 | 30.0 | 26.5 | 31.5 | 38.2 | 46.5 | 40.6 | 38.8 | 44.5 | 52.2 | 47.2 | 44.2 | 50.7 | 58.5 | 53.2 |
| MPs/DMBs | 8.05 | 5.4 | 5.67 | 7.92 | 4.58 | 3.56 | 3.0 | 3.2 | 3.14 | 2.64 | 2.35 | 2.98 | 3.0 | 2.32 | 2.12 | 2.13 |
| 2MP/3MP | 1.87 | 1.83 | 1.73 | 1.64 | 1.75 | 1.51 | 1.37 | 1.41 | 1.88 | 1.72 | 1.52 | 1.52 | 1.66 | 1.45 | 1.34 | 1.38 |
| 23DMB/22DMB | 1.0 | 0.75 | 0.6 | 0.66 | 0.84 | 0.71 | 0.8 | 0.70 | 0.73 | 0.77 | 0.76 | 0.94 | 0.8 | 0.81 | 0.72 | 0.61 |
| 2MP/23DMB | 10.5 | 8.2 | 9.6 | 12.3 | 6.36 | 5.16 | 3.91 | 4.5 | 4.84 | 3.82 | 3.27 | 3.72 | 4.25 | 3.0 | 2.91 | 3.26 |
| DMB selectivity | 9.7 | 13.7 | 13.3 | 9.43 | 15.2 | 18.8 | 21.7 | 19.7 | 20.1 | 23.1 | 25.6 | 20.5 | 20.3 | 25.0 | 27.3 | 25.7 |
| I/C | 7.24 | 7.5 | 8.0 | 5.3 | 5.7 | 6.2 | 6.75 | 4.8 | 4.96 | 5.3 | 6.15 | 4.5 | 4.5 | 4.96 | 5.88 | 4.21 |

decreasing trend observed in BET surface area (table 1) on increasing Ni addition.

### 3.2. Catalytic studies

The *n*-hexane and *n*-heptane hydroisomerization reactions were carried out separately over the reduced catalysts at LHSV = 1.33/h in the temperature range 225–375 °C in steps of 50 °C. The product distributions for *n*-hexane and *n*-heptane hydroisomerization are presented in tables 2 and 3, respectively. It is invariably found that 2-methyl pentane (2MP), 3-methyl pentane (3MP), 2,3-dimethyl butane (23DMB) and 2,2-dimethyl butane (22DMB) are the major products in *n*-hexane hydroisomerization and 2-methyl hexane (2MH), 3-methyl hexane (3MH), 3-ethyl pentane (3EP), 2,3-dimethyl pentane (23DMP), 2,4-dimethyl pentane (24DMP), 2,2-dimethyl pentane (22DMP), 3,3-dimethyl pentane (33DMP) and 2,2,3-trimethyl butane (223TMB) are the major products in *n*-heptane hydroisomerization. The formation of these products indicates the predominance of skeletal rearrangement in both *n*-hexane and *n*-heptane isomerization. Smaller amounts of cyclized, cracked and aromatized products were observed irrespective of the catalyst and reaction conditions.

The effect of temperature on *n*-hexane and *n*-heptane conversion over all the catalytic systems is shown in figures 3(a) and 3(b), respectively. It is found that both the *n*-hexane and *n*-heptane conversion increases with increasing temperature over all the catalytic systems. The maximum conversions of *n*-hexane and *n*-heptane over all the catalytic systems are observed at 375 °C for

Table 3
Product distribution of *n*-heptane hydroisomerization at various temperatures (LHSV = 1.33/h, mass of catalyst = 1.5 g, $H_2$ flow = 20 ml/min/g, time on stream = 1 h)

| Product | 225 °C | | | | 275 °C | | | | 325 °C | | | | 375 °C | | | |
|---|---|---|---|---|---|---|---|---|---|---|---|---|---|---|---|---|
| | $A_1$ | $A_2$ | $A_3$ | $A_4$ | $A_1$ | $A_2$ | $A_3$ | $A_4$ | $A_1$ | $A_2$ | $A_3$ | $A_4$ | $A_1$ | $A_2$ | $A_3$ | $A_4$ |
| 2MH | 9.0 | 9.7 | 12.6 | 11.0 | 12.0 | 13.6 | 15.3 | 14.8 | 13.0 | 15.0 | 16.0 | 15.2 | 13.3 | 15.8 | 15.5 | 15.0 |
| 3MH | 6.5 | 7.8 | 10.5 | 8.3 | 9.3 | 11.0 | 12.5 | 11.7 | 11.0 | 12.5 | 12.3 | 12.0 | 12.0 | 13.5 | 12.3 | 12.5 |
| 3EP | – | – | – | – | 1.0 | 1.4 | 2.0 | 1.5 | 1.5 | 2.0 | 2.3 | 1.0 | 2.0 | 2.5 | 2.0 | 1.5 |
| 23DMP | 1.0 | 2.0 | 3.2 | 2.5 | 3.2 | 4.0 | 6.0 | 3.8 | 4.2 | 5.0 | 6.7 | 4.3 | 5.0 | 5.8 | 7.5 | 5.3 |
| 24DMP | 0.5 | 1.0 | 2.0 | 1.0 | 1.5 | 2.3 | 3.5 | 2.3 | 2.0 | 2.8 | 4.3 | 3.0 | 3.2 | 4.0 | 5.1 | 3.8 |
| 22DMP | – | 1.0 | 1.0 | 0.5 | 1.0 | 1.5 | 2.0 | 1.0 | 1.5 | 2.0 | 2.6 | 2.0 | 2.0 | 2.7 | 3.8 | 2.3 |
| 33DMP | – | – | – | – | – | 0.5 | 0.5 | 0.5 | 0.5 | 1.0 | 1.5 | 1.0 | 0.5 | 1.0 | 1.8 | 1.5 |
| 223TMB | – | – | – | – | – | – | – | – | – | – | – | – | – | 0.5 | 1.0 | 0.5 |
| Others | 2.5 | 3.0 | 4.0 | 4.8 | 5.0 | 6.5 | 7.0 | 7.2 | 6.8 | 7.2 | 7.8 | 9.0 | 9.0 | 9.0 | 9.0 | 10.3 |
| Conversion (wt%) | 19.5 | 24.5 | 33.3 | 28.1 | 33.0 | 40.8 | 48.8 | 42.8 | 40.5 | 47.5 | 53.5 | 47.5 | 47.0 | 54.9 | 58.0 | 52.7 |
| 2H/3H | 1.38 | 1.24 | 1.2 | 1.32 | 1.33 | 1.23 | 1.22 | 1.26 | 1.18 | 1.22 | 1.3 | 1.26 | 1.10 | 1.17 | 1.26 | 1.2 |
| Mo/Mu | 10.3 | 4.3 | 3.7 | 4.8 | 3.65 | 2.96 | 2.48 | 3.68 | 3.10 | 2.73 | 2.0 | 2.73 | 2.55 | 2.35 | 1.55 | 2.30 |
| 2MH/23DMP | 9.0 | 4.85 | 3.93 | 4.4 | 3.75 | 2.75 | 2.55 | 3.89 | 3.09 | 3.0 | 2.38 | 3.5 | 2.66 | 2.72 | 2.0 | 2.83 |
| Mu selectivity (%) | 7.7 | 16.3 | 18.6 | 14.2 | 18.1 | 20.3 | 24.5 | 17.7 | 20.2 | 22.7 | 28.2 | 21.6 | 22.7 | 25.6 | 33.1 | 25.4 |
| I/C | 6.8 | 7.16 | 7.32 | 4.8 | 5.6 | 5.27 | 5.97 | 4.94 | 4.95 | 5.6 | 5.85 | 4.27 | 4.22 | 5.1 | 5.44 | 4.11 |

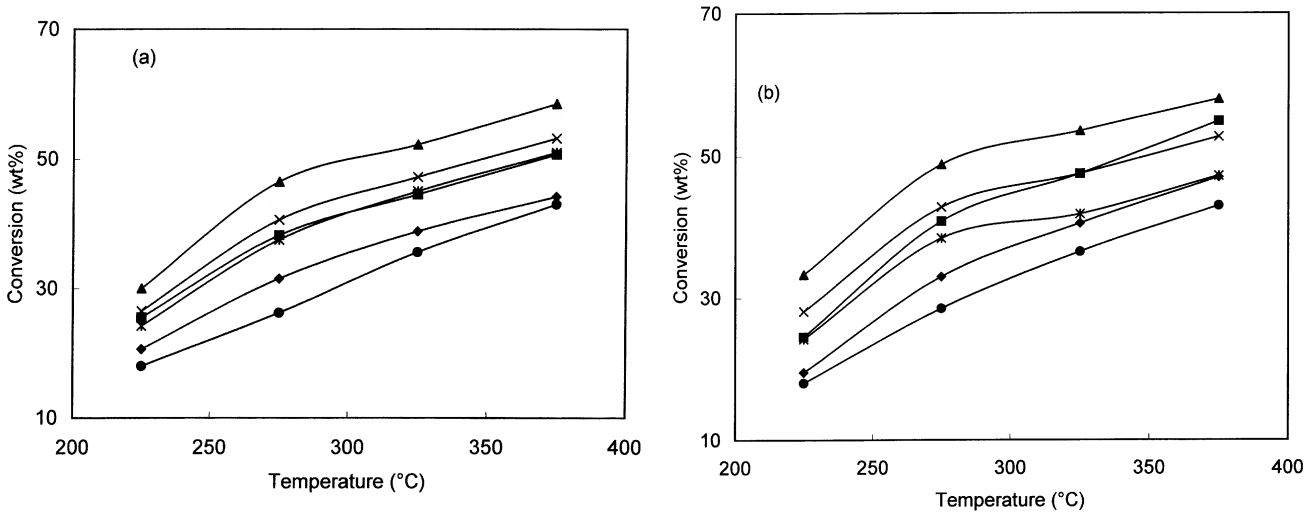


Figure 3. Effect of temperature on (a) *n*-hexane and (b) *n*-heptane hydroisomerization over various catalysts: (◆) $A_1$, (■) $A_2$, (▲) $A_3$, (×) $A_4$, (✳) $A_5$, (●) $A_6$.

the reaction temperatures studied. However, the isomerization selectivity in both *n*-hexane and *n*-heptane conversion over all the catalytic systems is found to decrease with increasing reaction temperature and is found to be a minimum at 375 °C. In the case of *n*-hexane, catalyst $A_1$ shows 20.6 wt% conversion with 87.8% isomerization selectivity at 225 °C. On increasing the temperature to 275, 325 and 375 °C, the *n*-hexane conversion is increased to 31.5, 38.8 and 44.2 wt% with corresponding isomerization selectivity of 85.0, 83.2 and 81.9%, respectively. Similarly, for *n*-heptane 19.5, 33.0, 40.5 and 47.0 wt% conversion with corresponding isomerization selectivity of 87.1, 84.8, 83.2 and 80.8% were observed at 225, 275, 325 and 375 °C, respectively, over catalyst $A_1$. It is observed that the *n*-hexane conversion is always higher than that of *n*-heptane at a fixed reaction temperature over all the catalytic systems.

The effect of Ni addition on *n*-hexane and *n*-heptane conversion can be studied by comparing the activity of Ni–Pt catalysts ($A_2$, $A_3$, $A_4$ and $A_5$) with that of Ni-free catalyst (catalyst $A_1$). The addition of 0.1 wt% Ni over catalyst $A_1$ increases the *n*-hexane conversion and isomerization selectivity significantly at all the temperatures studied. Catalyst $A_2$ shows 25.5, 38.2, 44.5 and 50.7 wt% *n*-hexane conversion with corresponding isomerization selectivity of 88.2, 86.1, 84.2 and 83.2% at 225, 275, 325 and 375 °C, respectively, which are significantly higher than that over catalyst $A_1$. The increasing trend in *n*-hexane conversion and isomerization selectivity with increasing Ni addition continues up to 0.3 wt% Ni addition. Maximum *n*-hexane conversion of 58.5 wt% with 85.4% isomerization selectivity was observed over catalyst $A_3$ at 375 °C. Further increase in Ni addition (catalyst $A_4$) leads to a decrease in conversion as well as isomerization selectivity at all the temperatures studied. Catalyst $A_4$ shows 26.5, 40.6, 47.2 and 53.2 wt% *n*-hexane conversion with 84.1, 82.7, 82.0 and 80.8% isomerization selectivity at 225, 275, 325 and 375 °C, respectively, which are considerably less than that over catalyst $A_3$.

In the case of *n*-heptane, maximum conversion of 52.7 wt% was observed over catalyst $A_3$ at 375 °C. The isomerization selectivity is also found to increase with increasing Ni addition up to 0.3 wt% similar to the observation made for *n*-hexane isomerization. Catalyst $A_3$ shows isomerization selectivity of 87.9, 85.6, 85.4 and 84.4% at 225, 275, 325 and 375 °C, respectively, which are considerably higher than that over catalyst $A_1$. Further increase of Ni addition (catalyst $A_4$) leads to a decrease in *n*-heptane conversion as well as isomerization selectivity. The maximum activity and selectivity observed on catalyst $A_3$ may be due to the better metal–acid synergism between bimetallic (Ni–Pt) particles as evidenced by TEM and the acid sites of the support. These particles are assumed as bimetallic (Ni–Pt) in nature. The TEM study shows that the average metal particle size of catalyst $A_3$ is 5.23 nm and the ESCA study confirms the complete reduction of Ni and Pt species, which are active in hydrogenation–dehydrogenation steps. The initial increase in conversion and isomerization selectivity in both *n*-hexane and *n*-heptane isomerization with increasing Ni addition up to 0.3 wt% can be accounted for in terms of the added Ni possibly increasing the number of active metallic sites, which increases the metallic sites/acid sites ratio towards the optimum value for the isomerization reaction [14]. A similar observation was already made by Jao *et al.* [24] that the addition of a moderate amount of Ni (0.5 wt%) to 0.2 wt% Pt/H-MOR enhances the conversion and rate of branched isomer formation and suppresses fuel gas formation in *n*-hexane and *n*-heptane hydroisomerization. On increasing the Ni addition to 1.5 wt%, a decrease in conversion and isomerization selectivity is observed. Further they surmised that the increase in metallic sites/acid sites ($N_M/N_A$) ratio by Ni addition is responsible for the observed enhanced

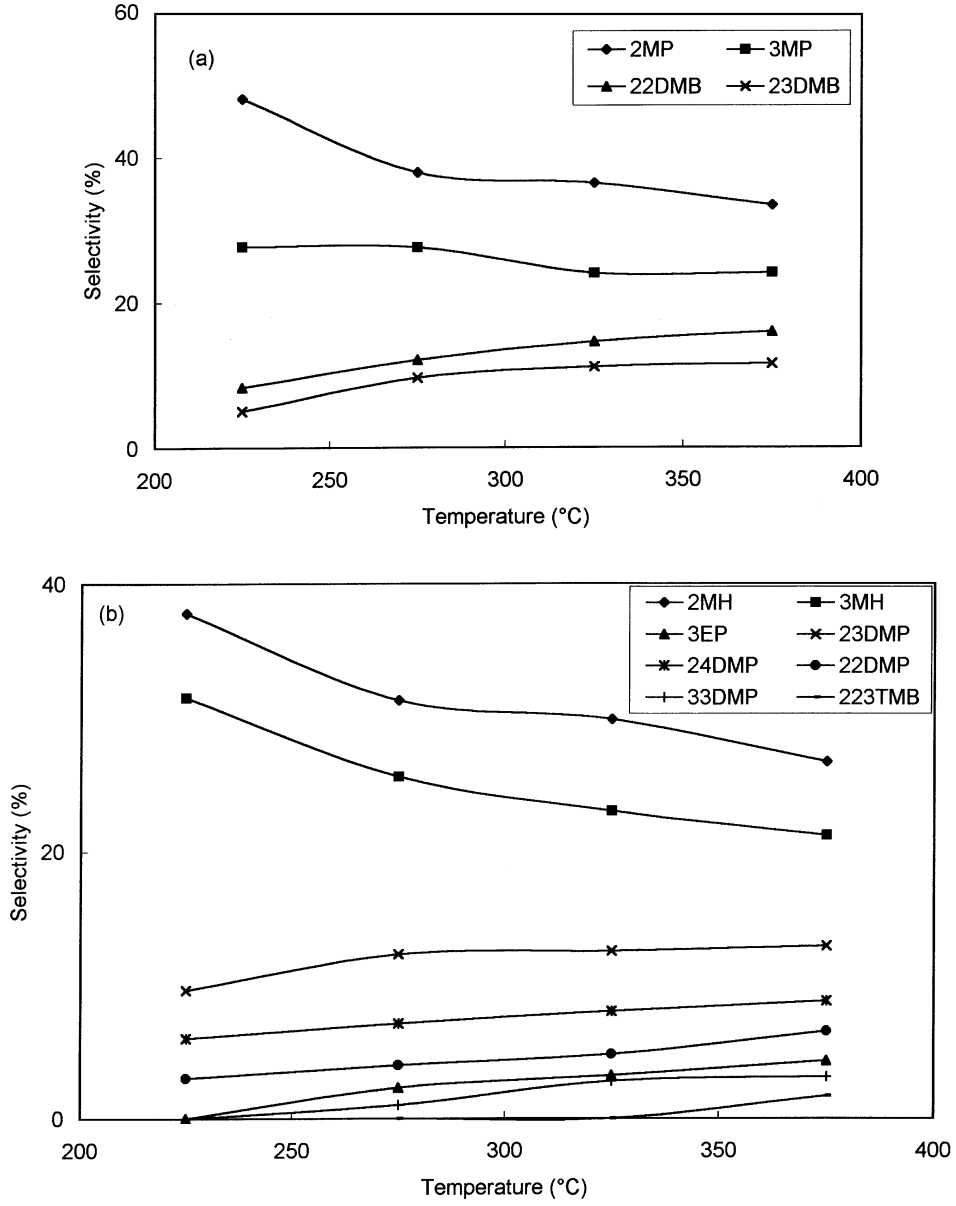


Figure 4. Effect of temperature on the selectivity of (a) hexane isomers and (b) heptane isomers over catalyst $A_3$.

activity of 0.5Ni–0.2Pt/H-MOR. Also in our previous study [27], 0.3Ni–0.1Pt/H-$\beta$ and 0.1Ni–0.1Pt/H-MOR showed an enhanced activity in *n*-hexane conversion, DMB selectivity and sustainability of the catalysts. Further addition of Ni leads to a decrease in conversion and DMB selectivity and is accounted for in terms of better synergism between catalytically active bimetallic (Pt–Ni) nanoparticles formed and acid sites of the supports. Similar observations were observed over 0.4 wt% Ni- and 0.2 wt% Pt-loaded SAPO-5 and SAPO-11 [28].

The effect of temperature on the selectivity of individual isomers of hexane and heptane over the best performing catalyst ($A_3$) is shown in figures 4(a) and 4(b), respectively. Among the four hexane isomers, the selectivity of 2MP is always found to be higher than 3MP, 23DMB and 22DMB at all the temperatures studied. The higher selectivity of 2MP compared to the other isomers indicates that 2MP is the precursor to the other isomers as reported in our previous studies [27,28]. The selectivity of 3MP is lower than that of 2MP. The higher selectivity of MPs compared with DMBs at all the temperatures studied indicates that monobranched isomers are primary reaction products even though the formation of 3MP is assumed to be a rapid 1,2 alkyl hydride shift in 2MP [34]. The selectivity of 2MP and 3MP is found to decrease and that of 23DMB and 22DMB increases with increasing reaction temperature. The decrease in 2MP selectivity is more than that of 3MP. A similar trend is observed over all other Ni–Pt ($A_2$, $A_4$ and $A_5$), Pt ($A_1$) and Ni ($A_6$) catalysts. The increasing DMB selectivity with decreasing MP selectivity with temperature increase indicates

the transformation of MPs to DMBs on increasing the temperature.

In the case of heptane isomers (figure 4(b)), the 2MH selectivity is found to be always higher than that of the other isomers. On increasing the temperature, the selectivity of monobranched isomers (2MH and 3MH) decreases and the decrease is much faster for 2MH than 3MH. A rapid 1,2 methyl shift is assumed to be responsible for the interconversion of 2- and 3MHs. Also, the selectivity of dibranched isomers 23DMP, 24DMP, 22DMP and 33DMP increases with increasing temperature. Among the dibranched isomers, the selectivity of 23DMP and 24DMP is found to be higher than that of 22DMP and 33DMP. The tribranched isomer 223TMB appears only at 375 °C. 33DMP and 3EP do not appear at lower (225 °C) temperature over all the catalysts. The increase in dibranched isomer formation with increasing temperature indicates that the dibranched isomers are secondary products formed from primary monobranched products. A similar trend in isomer selectivity is observed over all the other catalysts. The increase of multibranched isomer formation and decrease of monobranched isomer formation with increasing temperature suggests the transformation of monobranched into dibranched and dibranched to tribranched isomers with increasing temperature.

The effects of Ni addition on the ratios among the hexane and heptane isomers at various temperatures are presented in tables 2 and 3, respectively. In the case of hexane, it is observed that the MPs/DMBs ratio is found to decrease with Ni addition and the decrease is continued up to 0.3 wt% Ni at all the temperatures studied, *i.e.* high-octane DMB formation is enhanced by 0.3 wt% Ni addition. The MPs/DMBs ratios over catalyst $A_3$ are 5.67, 3.0, 2.35 and 2.12 at 225, 275, 325 and 375 °C, respectively, which is an opposite trend to the extrapolated thermodynamic equilibrium values (2.35 at 225 °C and 4.1 at 375 °C) of Condon [36] and Chen *et al.* [37]. Further Ni addition ($A_4$) leads to an increase in the MPs/DMBs ratio, *i.e.* a decrease in high-octane DMB formation. Similarly, in the case of heptane, the monobranched/multibranched (Mo/Mu) ratio is also found to decrease with increasing Ni addition up to 0.3 wt% and increases thereafter. The Mo/Mu ratios over the best performing catalyst ($A_3$) are 3.7, 2.48, 2.0 and 1.55 at 225, 275, 325 and 375 °C, respectively, which are much different from the thermodynamic equilibrium value (0.62 at 350 °C) reported by Vazquez *et al.* [23]. The increasing selectivity of multibranched isomers in both *n*-hexane and *n*-heptane hydroisomerization up to 0.3 wt% Ni addition may due to the favoring of a monomolecular mechanism by better metal–acid synergism between the catalytically active bimetallic (Ni–Pt) particles of nanometer scale formed and acid sites of the support. The TEM study of catalyst $A_3$ shows that the average particle size is 5.23 nm. Also, the ESCA study of catalyst $A_3$ shows the complete reduction of Pt and Ni cations to the metallic state which are active in the hydrogenation–dehydrogenation steps of hydroisomerization. The decrease in multibranched isomer formation over catalyst $A_4$ may be due to the formation of larger-sized (8.3 nm) bimetallic particles as well as unreduced Ni as evidenced by TEM and ESCA studies, respectively, which disturbs the better metal balance leading to poor activity. The catalysts with higher average particle size may hinder the movement of bulky intermediate in the pores of zeolite-Y. The pore size of Y-zeolite is 7.4 Å. The kinetic diameters of *n*-hexane, MPs, DMBs, *n*-heptane, MHs and DMPs are found to be 4.3, 5.5, 6.2, 4.9, 5.6 and 7.0 Å, respectively. More hindrance to the movement of multibranched isomers is expected in catalysts with larger-sized bimetallic particles. Hence, the multibranched isomer selectivity is less over catalyst $A_4$ with greater (8.3 nm) average particle size.

The 2MP/3MP ratios on catalyst $A_3$ are 1.73 and 1.34 at 225 and 375 °C, respectively, which are very close to the thermodynamic equilibrium ratios (1.70 at 225 °C and 1.45 at 375 °C) [35,37]. The 2MH/3MH ratios on catalyst $A_3$ are found to be 1.26 and 1.14 at 225 and 375 °C, which are also close to the thermodynamic equilibrium value (0.81 at 350 °C) [23]. The closeness of both 2MP/3MP and 2MH/3MH to the thermodynamic equilibrium ratios indicates that the 1,2 alkyl hydride shift involved in the interconversion of both 2MP and 3MP and 2MH and 3MH is extremely rapid [1,37]. The 23DMB/22DMB ratios over catalyst $A_3$ are 0.6 and 0.72 at 225 and 375 °C, respectively, which are close to the thermodynamic equilibrium ratios (0.55 at 225 °C and 1 at 375 °C) at lower temperature. The deviations at higher temperature may be due to the suppression of 22DMB formation by the difficulty involved in the transition of the more stable tertiary 2,3-dimethylbutyl carbocation to the less stable secondary 2,2-dimethylbutyl carbocation. Also, the direct transformation between methyl pentanes and 23DMB was reported by Daage and Fajula [38] from their $^{13}C$-labeled study on *n*-hexane isomerization and cracking.

Blomsma *et al.* [14] reported that 22DMB cannot be formed by the dimerization–cracking (bimolecular) mechanism. However, a considerable amount of 22DMB is observed over all the catalysts at all the temperatures studied. Hence, the *n*-hexane isomerization is considered to follow the mechanism of carbenium ion rearrangement and cleavage. According to the comprehensive rules of Brouwer [39] for carbenium ion rearrangement, carbenium ion isomerizations leading to a change in the degree of branching occur through protonated cyclopropane ring intermediates. Hence the 2MP/23DMB and 2MH/23DMP ratios are an indication of the rate of branching of hexane and heptane, respectively, by the protonated cyclopropane (PCP) intermediate formation mechanism, which is slower than the alkyl hydride shift mechanism according to Marin and Froment [40]. It is

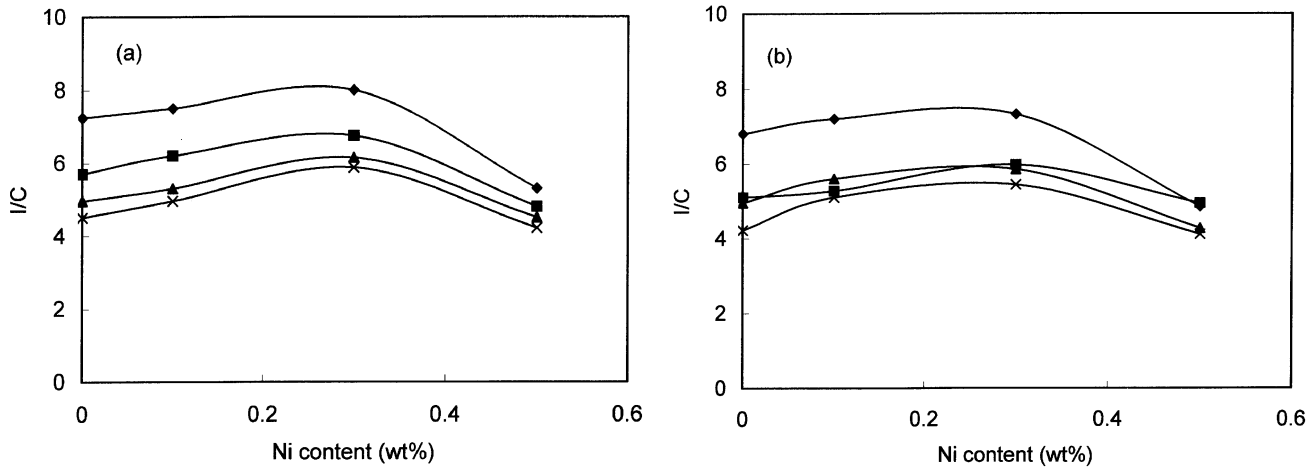


Figure 5. Effect of Ni addition on the I/C ratio of catalysts in (a) *n*-hexane and (b) *n*-heptane hydroisomerization at various temperatures: (◆) 225 °C, (■) 275 °C, (▲) 325 °C, (×) 375 °C.

observed from tables 2 and 3 that the addition of Ni decreases both the 2MP/23DMB and 2MH/23DMP ratio up to 0.3 wt% and thereafter the ratio increases indicating the favoring of the PCP intermediate formation mechanism by Ni addition. The increase in 2MP/23DMB and 2MH/23DMP ratio over catalyst $A_4$ indicates that the catalyst with a high average metal particle size and unreduced Ni not favoring the PCP mechanism may be due to disruption of better metal–acid synergism. Further it is observed that the addition of Ni up to 0.3 wt% increases the multibranched isomer selectivity in both hexane and heptane isomerization at all the temperatures studied. Catalyst $A_3$ shows the maximum multibranched isomer selectivity of 27.3 and 33.1% at 375 °C in *n*-hexane and *n*-heptane hydroisomerization, respectively.

The suitability of any catalyst for isomerization reaction is measured by its isomerization/cracking (I/C) ratio. A good isomerization catalyst should have a very high I/C ratio. The effect of Ni addition on I/C ratio in *n*-hexane and *n*-heptane conversion at various temperatures is shown in figures 5(a) and 5(b), respectively. It is observed that increasing Ni addition up to 0.3 wt% increases the I/C ratio, which decreases thereafter. The enhanced isomerization selectivity of catalyst $A_3$ may be accounted for in terms of its better metal–acid balance, bimetallic (Ni–Pt) nanoparticle formation and complete reduction of Ni and Pt species.

A time-on-stream study for a period of 6 h at 375 °C was carried out over the catalysts for the reactions in order to study the sustainability of the catalysts. All the catalysts show a decrease in conversion with time in both reactions. Here also, catalyst $A_3$ shows the least decrease compared with the other catalysts. Catalysts $A_1$ and $A_6$ show a rapid decrease in both *n*-hexane and *n*-heptane hydroisomerization with time. The rapid decrease in activity can be accounted for in terms of coke formation due to more cracking, which may occupy the active sites leading to lower activity.

## 4. Conclusion

The TEM images of Ni–Pt/H-Y zeolite catalysts show the formation of bimetallic (Ni–Pt) particles of nanometer scale. Also, it is found that the average particle size of bimetallic particles increases with increasing Ni loading. The XPS study on Ni–Pt/H-Y reveals that complete reduction of Ni occurs up to 0.3 wt% and further Ni addition leads to the occurrence of unreduced Ni as $NiAl_2O_4$. The acidity measurements of Ni–Pt/H-Y by $NH_3$-TPD and pyridine-adsorbed FTIR spectroscopy studies show that the increasing addition of Ni decreases the total acidity of the catalysts but does not affect the acidic strength of Ni–Pt/H-Y catalysts. Because of the best synergistic effect, the 0.3 wt% Ni–0.1 wt% Pt/H-Y catalyst shows an enhanced activity in both *n*-hexane and *n*-heptane hydroisomerization. Further Ni addition leads to a decrease in activity. Also, the 0.3 wt% Ni addition enhanced the multibranched isomer selectivity, protonated cyclopropane intermediate formation mechanism and sustainability of the catalysts in both *n*-hexane and *n*-heptane hydroisomerization. The enhanced activity of 0.3 wt% Ni–0.1 wt% Pt/H-Y may be due to better metal–acid balance, formation of catalytically active bimetallic (Ni–Pt) particles of nanoscale size and complete reduction of Ni and Pt species.

## Acknowledgment

The authors gratefully acknowledge the financial support from the Department of Science and Technology (DST), New Delhi, India.

## References

[1] G.E. Giannetto, G.R. Perot and M.R. Guisnet, Ind. Eng. Chem. Prod. Res. Dev. 25 (1986) 481.

[2] M. Guisnet, V. Fouche, M. Belloum, J.P. Bournonville and C. Travers, Appl. Catal. 71 (1991) 283.
[3] J.K. Lee and H.K. Rhee, Catal. Today 38 (1997) 235.
[4] J.K. Lee and H.K. Rhee, Korean J. Chem. Eng. 14 (1997) 451.
[5] E. Iglesia, S.L. Soled and G.M. Kramer, J. Catal. 144 (1993) 238.
[6] M.A. Arribas, F. Marquez and A. Martinez, J. Catal. 190 (200) 309.
[7] P.B. Weisz, Adv. Catal. 13 (1962) 137.
[8] C. Corolleur, D. Tomanova and F.G. Gault, J. Catal. 24 (1972) 401.
[9] J.R. Anderson and N.R. Avery, J. Catal. 7 (1967) 315.
[10] W.C. Kaag and R.M. Dessau, in: *Proc. 8th Congress on Catalysts*, Vol. 2 (Verlag Chemie, Weinheim, 1984) p. 305.
[11] Tiong Sie, Ind. Eng. Chem. Res. 31 (1992) 1881.
[12] H.Y. Chu, M.P. Rosynek and J.H. Lunsford, J. Catal. 178 (1998) 352.
[13] E. Blomsma, J.A. Martens and P.A. Jacobs, J. Catal. 155 (1995) 141.
[14] E. Blomsma, J.A. Martens and P.A. Jacobs, J. Catal. 165 (1997) 241.
[15] F. Fajula, M. Boulet, B. Cop, V. Rajafanova and T. Des Courieres, in: *Proc. 10th Int. Congress on Catalysis*, Budapest, eds. L. Guczi, F. Solymosi and P. Telenyi (Elsevier, Amsterdam, 1993) p. 1007.
[16] J.M. Compelo, F. Latont and J.M. Marinas, J. Catal. 156 (1995) 11.
[17] M. Hochtl, A. Jentys and H. Vinek, J. Catal. 31 (1999) 271.
[18] M. Hochtl, A. Jentys and H. Vinek, J. Catal. 190 (2000) 419.
[19] A.K. Sinha and S. Sivasankar, Catal. Today 49 (1999) 293.
[20] M.J. Girgis and Y. Peter Tsao, Ind. Eng. Chem. Res. 35 (1996) 386.
[21] K. Chaudhari, T.K. Das, A.J. Chandwadkar and S. Sivasankar, J. Catal. 189 (1999) 81.
[22] J.W. Ward, Fuel Process. Technol. 32 (1993) 55.
[23] I.M. Vazquez, A. Escardino and A. Corma, Ind. Eng. Chem. Res. 26 (1987) 1495.
[24] R.M. Jao, T.B. Lin and J.R. Chang, J. Catal. 161 (1996) 222.
[25] R.V. Malyala, C.V. Rode, M. Arai, S.G. Hegde and R.V. Chaudhari, Appl. Catal. A: General 193 (2000) 71.
[26] M.A. Jordao, V. Simoes, A. Montres and D. Cardoso, Stud. Surf. Sci. Catal. 130 (2000) 2387.
[27] I. Eswaramoorthi and N. Lingappan, Korean J. Chem. Eng. 20 (2003) (in press).
[28] I. Eswaramoorthi and N. Lingappan, Appl. Catal. A: General (in press).
[29] A. Lugstein, A. Jentys and H. Vinek, Appl. Catal. A: General 152 (1997) 93.
[30] K.H.W. Rohschlager, C.A. Emeis and K.A. van Santen, J. Catal. 86 (1983) 1.
[31] J.C. Bertolini, B. Tardy, M. Abon, J. Billy, P. Delichere and J. Massardier, Surf. Sci. 135 (1983) 117.
[32] C.H. Minchev, V. Knazirev, L. Kosova, V. Pechev, W. Grunsser and F. Schimidt, in: *Proc. 5th Int. Conf. on Zeolites*, ed. L.V.C. Rees (Heyden, London, 1980) p. 335.
[33] S. Narayanan, Zeolite 4 (1984) 231.
[34] P. Canizares, A. de Lucas, F. Dorado, A. Duran and I. Asencio, Appl. Catal. A: General 169 (1998) 137.
[35] L.-J. Leu, L.-Y. Hou, B.-C. Kang, C. Li, S.-T. Wu and J.-C. Wu, Appl. Catal. 69 (1991) 49.
[36] F.E. Condon, Catalysis 6 (1954) 1.
[37] J.K. Chen, A.M. Martin, Y.G. Kim and V.T. John, Ind. Eng. Chem. Res. 27 (1983) 401.
[38] M. Daage and F. Fajula, J. Catal. 81 (1983) 394.
[39] D.M. Brouwer, *Chemistry and Chemical Engineering of Catalytic Processes*, eds. R. Prins and G.C.A. Schult (Sijthof and Noordhoff, Germantown, MD, 1980).
[40] G.B. Marin and G. F. Froment, Chem. Eng. Sci. 37 (1982) 759.